Photoresponsive Surfactants for Controllable and Reversible Emulsion Systems

Hongyan Xue[1], Youmei Han[1], Guanglei Liu[1], Wenjing Chen[1], Zhihang Wang[2]*, and Nong Wang[1]*

[1] School of Chemistry and Chemical Engineering, Lanzhou Jiaotong University, Lanzhou, 730070, People's Republic of China

[2] School of Engineering, College of Science and Engineering, University of Derby, Markeaton Street, Derby DE22 3AW, UK

Abstract: Surfactants play a crucial role in applications such as oil-water separation, foam flotation, drug delivery, emulsion polymerization, and emulsifier recovery. Stimulus-responsive surfactants, as innovative smart materials, can reversibly control emulsion decomposition or phase transformation, facilitating emulsion circulation and component recovery. In this paper, two short-chain fluoroazobenzene photoresponsive surfactants (**FADC-2** and **FADC-4**) were synthesized. Three different reversible emulsion systems were constructed, leveraging the excellent chemical stability and rapid photoresponse of azobenzene and the trifluoromethyl group as a hydrophobic moiety. The results indicate that under different light exposures, the **FADC-2**/n-hexane/water and **FADC-4**/n-hexane/water emulsions exhibit reversible emulsification and demulsification cycles, while the **FADC-4**/n-octanol/water emulsions show reversible phase transfer. These findings highlight the effectiveness of photoresponsive surfactants in controlled emulsion systems, offering promising applications in fields requiring precise emulsion manipulation and liquid-liquid phase transfer, at the same time advancing the development of environmentally friendly, practical, durable, and stimulus-responsive surfactants.

KEYWORDS: Photoswitches; Azobenzene; Photoresponsive surfactant; Emulsion breaking

1. Introduction

Amphiphilic surfactants are used to generate various well-defined self-assembly micelles with controlled morphologies and sizes over nano- to micron-length scales.[1] These surfactants can stabilize interfaces and nanostructures,[2, 3] influencing solubilization, morphology, and biological, physical, optoelectronic, and chemical properties, offering a broad range of applications in materials science, organic synthesis, biomedicine, analytical chemistry.[4-6] On an industrial scale, surfactants also play a crucial role in the petroleum industry, particularly in enhancing the efficiency of oil recovery.[7-9] Compared with traditional surfactants, stimulus-responsive surfactants show unique value in the field of energy production and utilization because of their ability to control interfacial activity through external stimuli. Hence, stimulus-responsive emulsion systems prepared by stimulus-responsive surfactants can be used for reversible control of emulsion demulsification or phase conversion, facilitating emulsion circulation application and component recovery.[10-15] Different stimulus-response methods have unique advantages, but also present certain challenges. For example, pH[16] and N_2/ CO_2[17] stimulus-response emulsions are simple, convenient, and energy-efficient, however they introduce foreign substances into the system, affecting its composition and stability. Temperature-responsive emulsions[18] do not introduce foreign substances but require significant energy supplies for large-scale use. Similarly, magnetic field-responsive emulsions[19] avoid introducing foreign substances but necessitate special equipment and conditions, thereby increasing implementation complexity. Hence, developing controllable and reversible emulsion systems based on innovative smart surfactants, without adding extra substances, with lower energy consumption, and simple accessibility, is essential.

In this context, the development of photoresponsive emulsion technology has the potential to meet the aforementioned requirements, while also promoting a green, circular, and low-carbon economy. Among various emulsion systems, controllable emulsions with photoresponsive surfactants offer several advantages, including easy application, rapid response, good repeatability, and non-contact control.[20-24] To design such system, photoswitchable molecules can be used as the foundation for developing photoresponsive surfactants. As one typical scaffold, azobenzene (AZO) shows great application potential due to its dual-light control switch, tunable thermal half-life, and stability.[25] In recent years, applications of AZO in solar energy storage,[26] drug-delivery systems,[27] bioimaging,[28] oil-water separation,[29] adhesion,[30] and liquid crystals[31] have been extensively investigated. Structurally, the parent molecule typically undergoes a UV light-triggered transition from a thermally stable, apolar *trans* configuration to a bent, polar *cis* configuration. The back conversion can be achieved *via* thermal kinetics or visible light irradiation.[25] Synthetically, AZO and its derivatives can be fairly easy made by various methods such as coupling reactions, Mills reaction, and Wallach reaction.[32] Therefore, AZO derivatives are considered as one of the most practical substituents for switchable emulsion system design.

On the other hand, to enhance the functionality of the surfactant, fluorinated substituents can be integrated into the molecule. Previously, it was found that fluorinated surfactants[33-36] possess unique chemical properties, particularly in polyfluorinated or perfluorinated structures with long chains.[37-39] For instance, these surfactants exhibit high hydrophobicity and low surface tension, making them widely used in industrial and agricultural production, daily life, and other fields.[40, 41] However, surfactants with a high number of fluorocarbon atoms are less biodegradable and highly water-soluble, allowing them to easily enter domestic water systems through rain, lakes, rivers, oceans, and soil, resulting in long-term potential environmental impacts.[42-45] To retain the performance advantages of fluorinated surfactants

while minimizing their environmental impact, previous research has explored the strategy of shortening their carbon chain length.[46, 47] Due to the high electronegativity of fluorine atoms, carbon-fluorine bonds exhibit strong polarity, allowing even shorter carbon-fluorine hydrophobic chains to maintain excellent hydrophobicity in water-based media. At the same time, shortening the carbon chain can accelerate the biodegradation rate of these surfactants, thereby reducing their environmental impact. Therefore, careful control of the carbon chain length is essential for balancing hydrophobicity and environmental friendliness.

In this study, two novel short-chain fluoroazobenzene photoresponsive surfactants (**FADC-2** and **FADC-4**) were successfully synthesized by combining the aforementioned two key substituents, with a focus on balancing performance optimization and environmental sustainability. To demonstrate the practical application potential, we constructed two photoresponsive phase separation emulsion systems (**FADC-2**/n-hexane/water and **FADC-4**/n-hexane/water), which exhibited excellent emulsion formation and breaking cyclability with precise control (up to 20 repeating cycles). Additionally, a phase transfer emulsion system was developed, where the surfactant (**FADC-4**/n-octanol/water) can be remotely controlled under dual-light irradiation to move between the aqueous phase and the organic phase. The results show that these newly developed emulsification systems have significant potential for efficient product separation and catalyst recovery, driving the development of recyclable and environmentally friendly emulsification technologies.

2. Experimental Section

2.1. Materials.

3,5-bis(trifluoromethyl)aniline (AR), sodium nitrite (AR), sodium hydroxide (AR), potassium bicarbonate (AR), potassium iodide (AR) and phenol (AR) were purchased from Shanghai Macklin Biochemical Technology Co., LTD. 1,2-Dibromoethane (AR) and 1,4-

dibromobutane (AR) were purchased from Tianjin Damao Reagent Co., LTD. Potassium carbonate (AR) and N,N-dimethylethanolamine (AR) were purchased from China Aladdin Biotechnology Co., LTD. n-Hexane was purchased from Tianjin Damao Reagent Co., LTD，n-Octanol was purchased from Nanjing Chemical Reagent Co., LTD.

2.2. Equipment and Characterization.

^{1}H NMR (500 MHz) spectra of all intermediate and final products were recorded on 500 Mhz NMR Spectrometer (Bruker Avance Neo 500) in deuterated dimethyl sulfoxide (DMSO-d_6, except for ***$(CF_3)_2$-AZO-OC_2H_4Br*** in deuterated chloroform, $CDCl_3$). All spectra were referenced internally relative to Tetramethylsilane ($SiMe_4$, δ = 0 ppm) using the residual solvent resonances. Coupling constants are reported in Hz.

The structures of all products were further confirmed by Fourier-transform infrared spectrometer (FTIR, Nexus 470) with a wavelength range of 4000 cm^{-1} to 400 cm^{-1} and a resolution of 4 cm^{-1}.

The final products of **FADC-4** were dissolved in ethyl acetate (1.5 g L^{-1}), and the corresponding absorption spectra were measured by ultraviolet-visible spectrophotometer (UV-Vis, Metash UV-5200PC).

The photoswitchable reactions of both surfactants were controlled with a 365 nm LED UV lamp (20 W) from *trans* to *cis* state, and a 445 nm LED visible lamp (20 W) from *cis* back to *trans* state.

Microscopy images were used to observe the particle size distribution of the **FADC-2**/n-hexane/water emulsion. The emulsion was quickly dropped onto a glass slide and irradiated with UV light from 4 cm above the slide. The process was monitored under the microscope and photographed. The emulsion type and particle size distribution were observed by fluorescence microscope (Olympus BX53) and optical microscope (Motic B Series).

2.3. Computational methods

Density functional theory (DFT) was employed to gain insights into the structural and electronic properties. All calculations were carried out with the Gaussian16 program[48] tightening both self-consistent field (10^{-10} a.u.) and geometry optimization (10^{-5} a.u.) convergence.

All UV–Vis absorption spectra of the monomers were computed using the time-dependent density functional theory (TD-DFT) method at the CAM-B3LYP/6-311+G(d,p) level of theory. The absence of any imaginary frequencies indicated that the molecules were located at their true minima on the potential energy surfaces.

2.4. Preparation methods

Two kinds of smart photoresponsive fluoroazobenzene surfactants: 2 - (4 - ((3, 5 - double (three fluorinated methyl) phenyl) diazo) phenoxy) - N - (2 - hydroxyethyl) - N, N - dimethyl ethane - 1 - ammonium bromide (named **FADC-2**), and 4-(4-((3, 5-bis (trifluoromethyl) phenyl) diazo) phenoxy)-N-(2-hydroxyethyl)-N, N-dimethyl butane-1-ammonium bromide (named **FADC-4**) were synthesized. Figure 1 outlines the synthesis route for the two smart photoresponsive fluoroazobenzene surfactants. The general synthesis mechanism is delineated into three primary steps: diazotization, nucleophilic substitution and quaternary amination reactions.

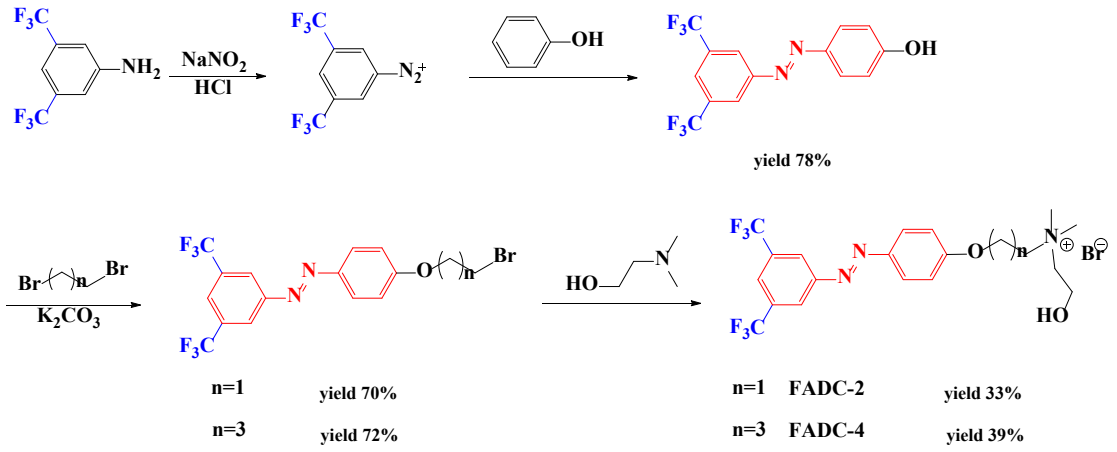

Figure 1. Synthesis route of two smart photoresponsive surfactants.

2.4.1. Synthesis of 3, 5-trifluoromethyl-4-hydroxy-azobenzene ($(CF_3)_2$-AZO-OH)

The whole reaction was carried out in an ice bath close to 0 °C. 25 mL of hydrochloric acid was added to a 1000 mL round-bottom flask, followed by the slow addition of 3,5-bis(trifluoromethyl)aniline (10 mL, 0.064 mol) to form a white crystal. Then, 100 mL of water was added to form a paste precipitate by stirring. Sodium nitrite (6.6 g, 0.096 mol) was dissolved in 30 mL of distilled water and poured into a 100 mL constant pressure dropping funnel. This solution was added to the above mixture at a rate of 1 drop per second over 30 minutes. After dissolution of the precipitate, the crude product was filtered to obtain reaction liquid A. Phenol (6 g, 0.064 mol) and sodium hydroxide (3 g, 0.075 mol) were dissolved in 40 mL of distilled water, and the pH was adjusted to 10 with dilute hydrochloric acid to obtain mixture B. Reaction liquid A was then slowly added to mixture B, maintaining the pH of the system at 8-10 using sodium hydroxide aqueous solution. After the addition, the mixture was stirred for 2 hours until the reaction was complete, and the pH of the solution was adjusted to neutral with dilute hydrochloric acid. The mixture was then filtered under reduced pressure and washed three times with distilled water. The crude product was purified by methanol, recrystallized with water, and collected. Finally, it was further purified by column chromatography (the volume ratio of ethyl acetate to petroleum ether was 1:5), the resulting ***$(CF_3)_2$-AZO-OH*** was collected as a yellow-colored powder and dried in a vacuum oven for 48 h (yield: 78 %).

2.4.2. Synthesis of 1-(3,5–double (trifluoromethyl) phenyl)-2-(4-(2-bromine ethoxy) phenyl) 2 nitrene ($(CF_3)_2$-AZO-OC_2H_4Br) and 1-(3, 5-double (trifluoromethyl) phenyl)-2-(4-(4-bromine butoxy) phenyl) 2 nitrene ($(CF_3)_2$-AZO-OC_4H_8Br)

1,2-Dibromoethane (2.7 mL, 0.0315 mol) was added to a 250 mL round-bottom flask along with sufficient potassium carbonate (about 15 g) and appropriate amount of acetone (ca. 50 mL). A small amount of potassium iodide (about 0.02 g) was then added. In a 100 mL

constant pressure funnel, azophenol (10 g, 0.03 mol) was mixed with acetone (80 mL). This mixture was gradually added to the round-bottom flask containing 1,2-dibromoethane. After the addition was complete, the mixture was refluxed at 75°C for 8 hours until the reaction was complete. The reaction mixture was then poured into deionized water and extracted with methylene chloride. The organic phase was collected, and the crude product was obtained by spin evaporation and drying, then was separated and purified by column chromatography (the volume ratio of ethyl acetate to petroleum ether was 1:40). The ***$(CF_3)_2$-AZO-OC_2H_4Br*** was collected as a yellow powder and dried in a vacuum oven for 48 hours, yielding 70%. The synthesis method for ***$(CF_3)_2$-AZO-OC_4H_8Br*** was similar. The crude product was separated and purified by column chromatography using a 1:20 volume ratio of ethyl acetate to petroleum ether, resulting in a yellow powder with a yield of 72%.

2.4.3. Synthesis of FADC-2 and FADC-4

The entire reaction was carried out in a nitrogen atmosphere. The obtained ***$(CF_3)_2$-AZO-OC_2H_4Br*** was mixed with an appropriate amount of acetonitrile in a round-bottom flask until fully dissolved. N,N-Dimethylethanolamine was then added in the same amount as ***$(CF_3)_2$-AZO-OC_2H_4Br***. The reaction progress was monitored by Thin Layer Chromatography (TLC) after heating and refluxing for three days. Upon completion of the reaction, the reaction mixture was cooled to room temperature, precipitating crystals. These crystals were filtered under reduced pressure, then heated and stirred with the minimum amount of dichloromethane until just dissolved. A large amount of cold petroleum ether was rapidly added to precipitate orange crystals. After recrystallization and drying, obtained the final product **FADC-2** with a yield of 33%. The synthesis method with ***$(CF_3)_2$-AZO-OC_4H_8Br*** for **FADC-4** was the same, and a yield of 39% was determined. Due to the synthesized azobenzene surfactants being easily adsorbed by silica gel during purification via column chromatography, they were instead separated and

purified through recrystallization. However, a significant portion of the product remained dissolved in the recrystallization solvent, leading to a lower yield.

2.4.4. Preparation of photoresponsive phase separation emulsion system FADC-2/ n-hexane/ water and FADC-4/ n-hexane/ water

A series of emulsions with different concentrations of surfactant **FADC-2** or **FADC-4** were prepared using H_2O as the water phase and n-hexane as the oil phase. These emulsions were stirred magnetically at room temperature for 5 minutes to form the emulsion systems. UV light was used to test for photoresponsive phase separation properties. The composition and proportion were adjusted until the desired photoresponsive phase separation property was achieved, thereby determining the optimal composition of the emulsion system.

2.4.5. Preparation of photoresponsive phase transfer emulsion in FADC-4/ n-octanol/ water system

Similar to part 2.3.4, a series of emulsions were prepared. Instead of n-hexane, n-octanol was used as the oil phase for **FADC-4**. 365 nm and 445 nm light sources were used to determine the photoresponsive surfactant phase transfer properties. Various compositions and proportions were tested until the optimal composition of the emulsion was found. **FADC-2/n-octanol/water** was also tested; however, an obvious phase transfer emulsion system was not observed.

3. Results and Discussion

3.1. Structural characterization of FADC-2 and FADC-4

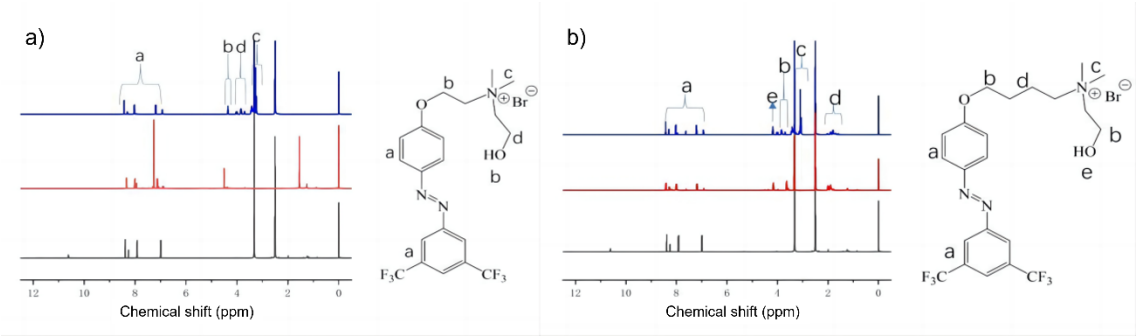

Figure 2. ^{1}H-NMR spectrum of monomers and surfactants. The black spectrum represents ***$(CF_3)_2$-AZO-OH***, the red spectrum represents a) ***$(CF_3)_2$-AZO-O$(CH_2)_2$Br*** and b) ***$(CF_3)_2$-AZO-O$(CH_2)_4$Br***, and the blue spectra represent final **FADC-2** and **FADC-4**, respectively.

The nuclear magnetic resonance (^{1}H-NMR) data of each step of synthesizing quaternary ammonium surfactant **FADC-2** and **FADC-4** were shown in Figure 2. Figure 2a shows the ^{1}H NMR spectrum of **FADC-2**, in which the characteristic peaks in aromatic hydrogen of azobenzene were obvious at chemical shifts of 7.19 ppm, 7.00 ppm, 8.04 ppm and 8.52 ppm, respectively. The methylene associated with oxygen has obvious characteristic peaks at chemical shifts of 3.43 ppm and 3.84 ppm. The characteristic peaks associated with saturated alkyl associated with N appear in the chemical shift range of 3.3-3.2 ppm. Compared with Figure 2b, an increase in the characteristic peaks associated with the unsaturated alkyl connected to N can be observed at chemical shifts of 1.88 ppm and 1.83-1.76 ppm, respectively.

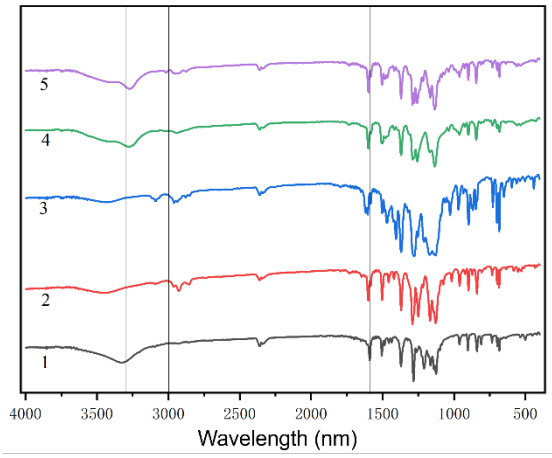

Figure 3. Infrared spectrum of 1: ***$(CF_3)_2$-AZO-OH***; 2: ***$(F_3C)_2$-AZO-OC_2H_4Br***; 3: ***$(F_3C)_2$-AZO-OC_4H_8Br;*** 4: **FADC-2** and 5: **FADC-4**.

Figure 3 shows the FTIR of azophenol (1), bromo-substituted azobenzene (2), quaternary ammonium salt (3) and the final produced (4: **FADC-2** and 5: **FADC-4**). It can be seen from the figure that the stretching vibration peak of -OH on the azophenol benzene ring is at 3385 cm^{-1}. With the reaction progress, -OH disappears and the -C-Br group and -CH_2- bond are introduced. Therefore, there was no stretching vibration peak at 3385 cm^{-1} in ***$(F_3C)_2$-AZO-Br***. The stretching vibration of ether bond appears at 1137cm^{-1}. At the same time, -C-H stretching vibration is present around 3000 cm^{-1}, C-F stretching vibration peak was present at 1063 cm^{-1}, benzene ring skeleton stretching vibration was present at 1592 cm^{-1}, in-plane bending vibration of -C-H was present at 1496 cm^{-1}, and out-of-plane bending vibration of substituted aromatics was present at 855 cm^{-1}. All their FTIR spectrum consistent with the target molecule.

3.2. Photo-responsiveness calculation of FADC-2 and FADC-4

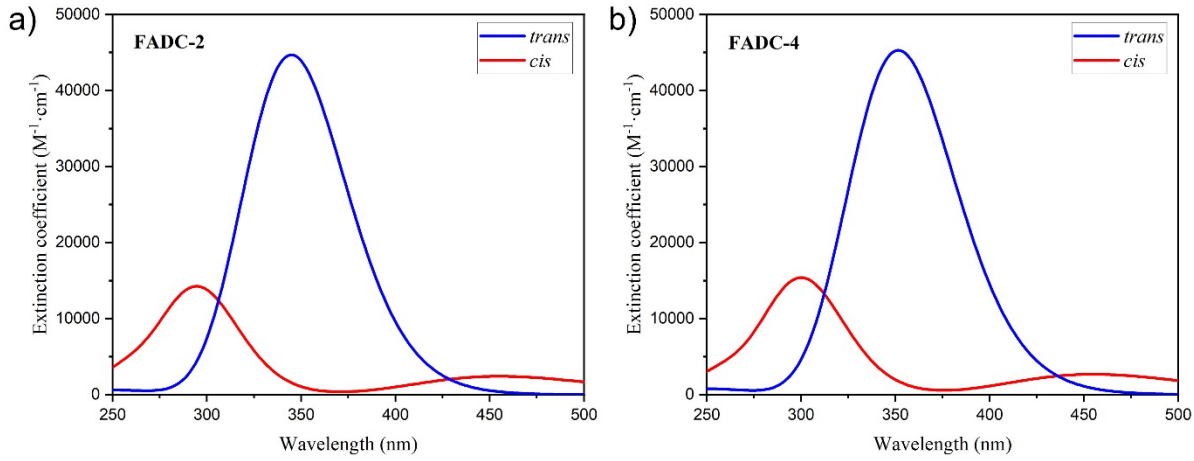

Figure 4. Theoretical UV-Vis absorption spectra of (a) **FADC-2** and (b) **FADC-4**.

Figure 4 shows the theoretical UV-Vis spectra calculations of the *cis-trans* conformation transformation of quaternary ammonium surfactants **FADC-2** (Figure 4a) and **FADC-4** (Figure 4b) in aqueous solution, performed using the DFT method. The calculated maximum absorption peaks for *trans* **FADC-2** and **FADC-4** are 351.4 nm and 344.4 nm, respectively.

For the *cis* form, **FADC-2** exhibits two maximum peaks at 294.0 nm and 455 nm, while **FADC-4** shows peaks at 299.6 nm and 455 nm.

3.3. FADC-2, FADC-4 emulsification and demulsification

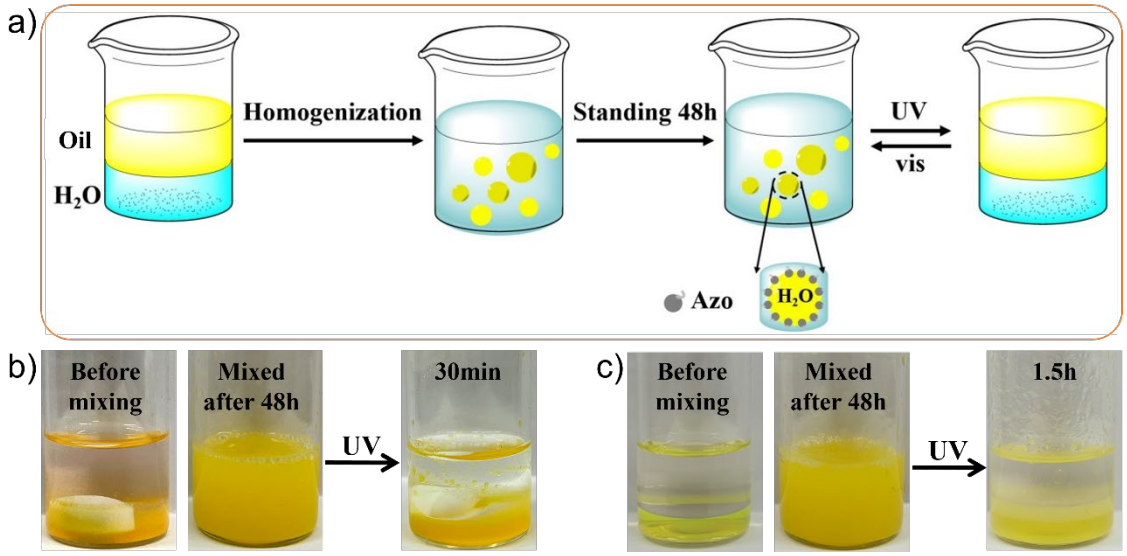

Figure 5. a) UV light emulsification demulsification process; b) **FADC-2**/n-hexane/water systems at 25°C; c) **FADC-4**/n-hexane/water systems at 25°C.

In order to study the effect of alkyl chain length on emulsification and demulsification performance of quaternary ammonium surfactant, 10 mmol/L **FADC-2** and **FADC-4** aqueous solutions (water mass fraction is 0.3) were prepared at 25°C. n-Hexane (with a mass fraction of 0.7) was then added, and the mixture was stirred for 5 minutes at 500 r/min to ensure thorough mixing of water, n-hexane, and the surfactants. The homogenized emulsion was left for 48 hours without breaking and stratified. DFT calculations show that **FADC-2** and **FADC-4** exhibit very similar *trans*/*cis* absorption spectra, with the maximum absorption of the *trans* state around 340 nm and the absorption peak for back-conversion from *cis* to *trans* state is around 440 nm. Therefore, the breaking time was recorded by irradiation with a 365 nm UV lamp (Figure 5a).

As can be seen from Figure 5b, the emulsion constructed by **FADC-2** surfactant can be photodemulsified after stirring and homogenizing, and only 30 min of ultraviolet irradiation is

needed to complete the photodemulsification, while the emulsion constructed by **FADC-4** surfactant can be demulsified after 1.5h (figure 5c). With the increase of hydrophilic group carbon chain, the demulsification time becomes longer and the demulsification rate slows down, it shows that increasing the length of carbon chain is not conducive to demulsification. The reason for this phenomenon may be that surfactants with longer alkyl chains are more capable of displacing surfactants in the oil. The increase of alkyl chain in the surfactant leads to the decrease of hydrophilicity of the surfactant, the decrease of the surfactant's tendency to dissolve and stay in the water droplets, and the decrease of the demulsification rate.

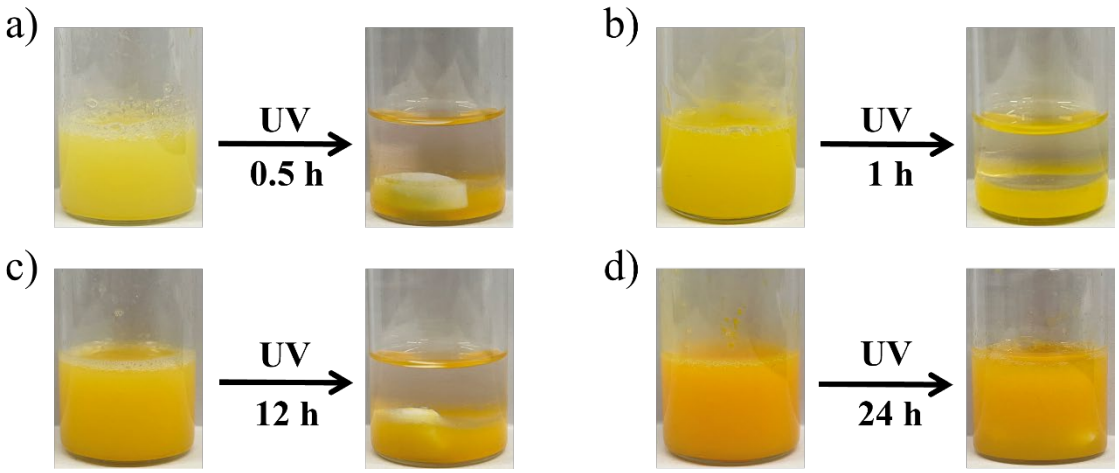

Figure 6. FADC-2/n-hexane/water emulsion system at 25°C with varying concentrations: a) 10 mmol/L; b) 20 mmol/L; c) 30 mmol/L; d) 50 mmol/L.

In order to further understand the effect of surfactant concentration on emulsion stability, **FADC-2**/n-hexane/water emulsion systems with different concentration of **FADC-2** was constructed. It can be observed from Figure 6 that when the concentration of **FADC-2** is 10 mmol/L, the demulsification can be completed in only 30 minutes; when the concentration is increased to 20 mmol/L, the demulsification time is 1h, doubling the time. When the concentration is 30 mmol/L, UV irradiation for up to 12 hours is required to break the emulsion. With the increase of surfactant concentration, the demulsification time also became longer. When the concentration was 50 mmol/L, the demulsification time remained unchanged for 24h

under ultraviolet light. According to the above experiments, increasing the concentration of surfactant aqueous solution will have an adverse effect on the demulsification of emulsion. When the concentration is too high, breaking emulsion may not occur, likely due to photostationary state of the AZO compounds. [49]

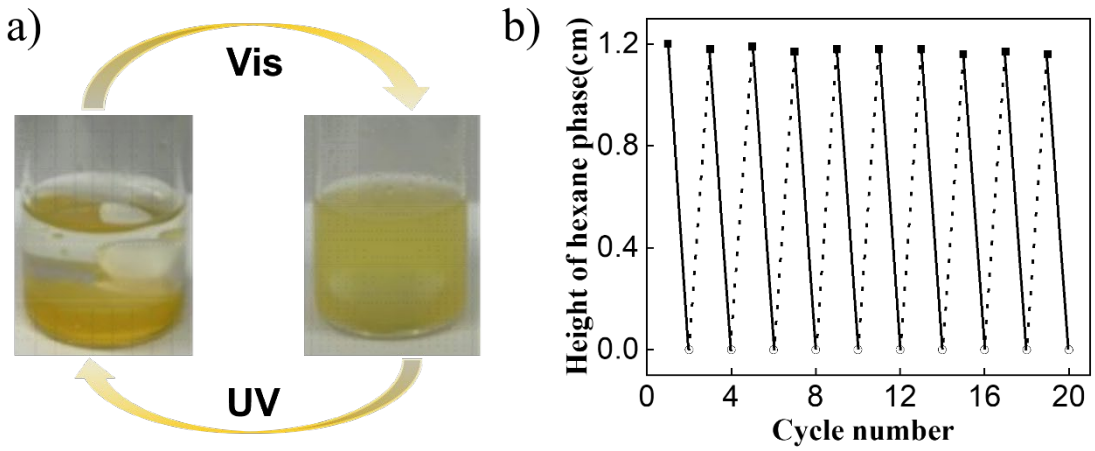

Figure 7. a) The **FADC-2**/n-hexane/water emulsion system demonstrated demulsification induced by alternating visible and UV light after 10 cycles, with the solution under constant stirring conditions during irradiation; b) Height change of the n-hexane phase during 10 repeated demulsification cycles of the **FADC-2**/n-hexane/water emulsion system (solid line: photoisomerization under ultraviolet irradiation; dotted line: photoisomerization under visible light irradiation).

For real-world applications, emulsion stability is crucial for maintaining its functionality.[50-53] To further study the cycling properties of the system, **FADC-2** was used to repeat the demulsification-emulsion loop. When the **FADC-2**/n-hexane/water emulsion system was irradiated with 365 nm UV light, the configuration of **FADC-2** changed from *trans* to *cis*, causing the emulsion to demulsify and stratify. After further irradiation with 445 nm blue light, **FADC-2** reverted from its cis configuration to trans, and the emulsion became a single phase again. After 10 repeated cycles, the system remained completely reversible (Figure 7a). Additionally, the height of the hexane phase was measured over 20 cycles, and no

clear change was observed, confirming stable phase separation over irradiation cycles (Figure 7b).

3.4. Photoresponsive phase separation emulsion FADC-2/ n-hexane/water system

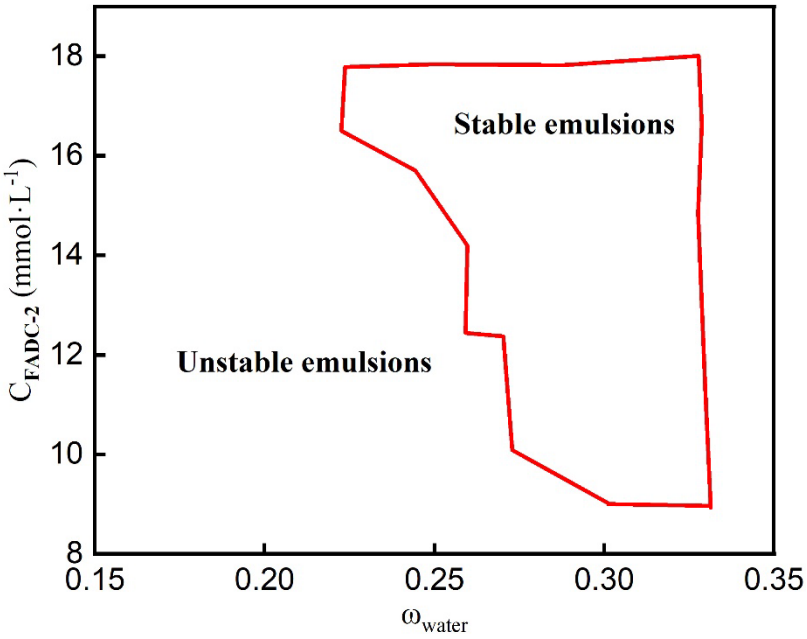

Figure 8. Phase diagram of the **FADC-2**/n-hexane/water stabilized emulsion system. The vertical axis represents the concentration of the **FADC-2** aqueous solution, while the horizontal axis indicates the mass fraction of the aqueous solution with varying concentrations of **FADC-2**.

To gain a comprehensive understanding of the constructed emulsion systems, the phase diagram of the **FADC-2**/n-hexane/water emulsion system was further studied and drawn. As shown in Figure 8, the emulsion within the irregular shape is a stable emulsion that can remain unstratified for 48 hours after homogenization, while the rest is an unstable emulsion with a minimum water mass fraction of 0.22 and a minimum aqueous concentration of **FADC-2** of 8.3 mmol/L. In the following study, we adopted the mass fraction of water as 0.30.

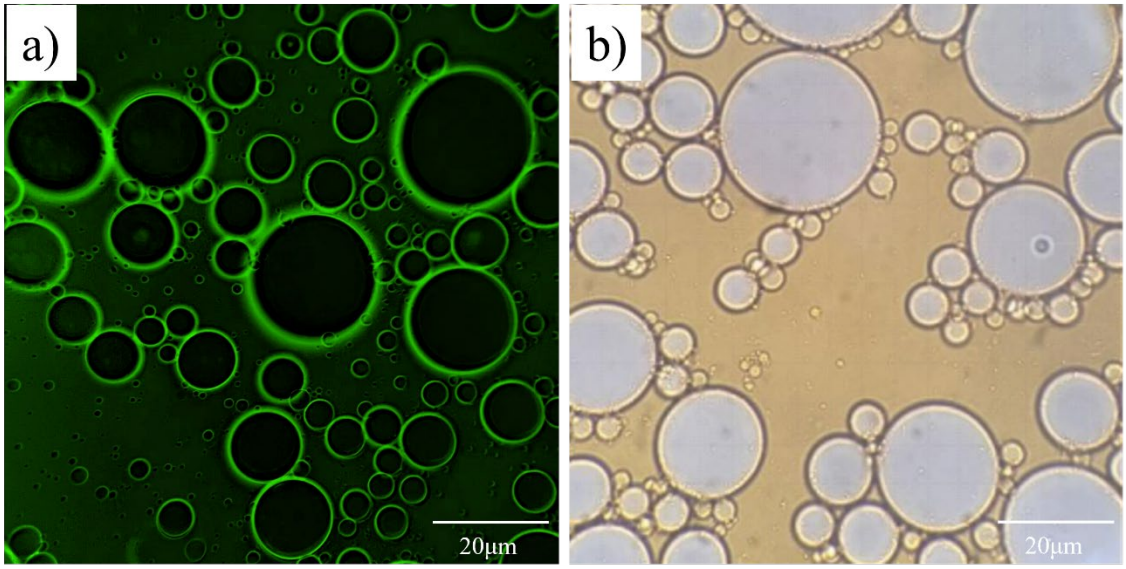

Figure 9. a) Fluorescein sodium-stained emulsion fluorescence micrograph; b) Optical micrograph of the **FADC-2**/n-hexane/water emulsion.

As shown in Figure 9, fluorescence microscopy was used to investigate the type of **FADC-2** /n-hexane/water emulsions. Figure 9a presents the fluorescence microscopic image of the emulsion, while Figure 9b shows its optical microscopic image. In this system, fluorescein dissolves only in the water phase, appearing green in the fluorescence images. The figure shows that the continuous phase of the emulsion is green, indicating that the emulsion is oil-in-water (O/W). This result is consistent with the findings from the dilution method, where adding water to the emulsion results in stratification or turbidity if it is oil-in-water. Therefore, the prepared intelligent photoresponsive emulsion system is confirmed to be oil-in-water.

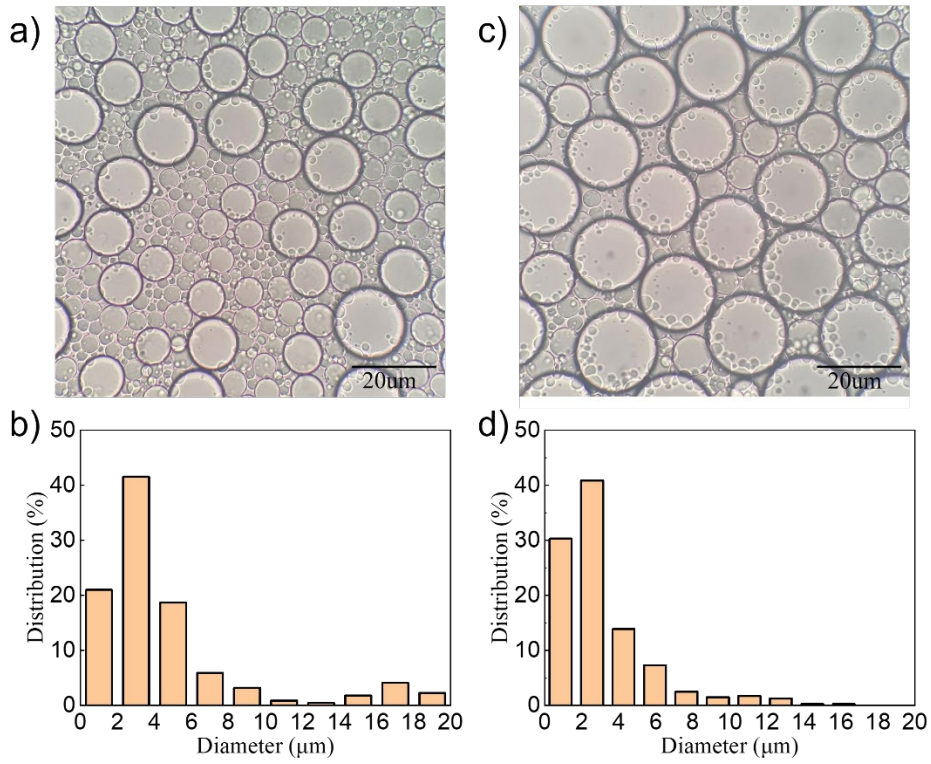

Figure 10. Microscopy images and particle size distributions of water droplets in an emulsion composed of n-hexane and azobenzene aqueous solutions (n-hexane: surfactant aqueous solution = 70:30): a, b) Before ultraviolet irradiation; c, d) After 10 minutes of ultraviolet irradiation.

According to the optical microscopic image of emulsions **FADC-2**/ n-hexane/water, and using the particle size analysis software Nano Measurer, the particle size distribution of water droplets dispersed in **FADC-2**/ n-hexane/water emulsion system was measured, as shown in Figure 10. It was found that the diameter of water droplets ranged from 0.73 μm to 16.3 μm, with an average diameter of 2.55 μm. After 10 minutes of ultraviolet irradiation, the particle size of the emulsion increased significantly. Larger water droplets increased, the diameter ranges of the water droplet change from 0.72 to 19.68 μm, the average particle size of the emulsion is 3 μm. The water droplet distribution of less than 2 μm decreases, and the particle size distribution of 15-20 μm increases. This shows that ultraviolet irradiation can make the water droplets grow larger, it can be inferred that with the increase of ultraviolet irradiation

time, the water droplets will continue to grow larger, and the oil phase will be connected together to achieve the transition of emulsification to demulsification.

This observation can be explained by the fact that surfactants with strong lipophilicity and weak hydrophilicity tend to form stable water-in-oil emulsions, while surfactants with strong hydrophilicity and weak lipophilicity are more likely to form stable oil-in-water emulsions. Since there is more oil than water, so the prepared photoresponsive system are water-in-oil emulsions. After ultraviolet irradiation, the azobenzene surfactant changed from trans isomer to cis-isomer, and the polarity of the molecule was enhanced. Our previous research has shown that non-woven fabric containing azobenzene polymer structure werer irradiated by UV, hydrophobic surface changed into hydrophilic surface.[29] Therefore, after ultraviolet irradiation, the hydrophilicity of azobenzene surfactants were also enhanced, which is not conducive to the formation of stable water-in-oil emulsion, resulting in demulsification. After further use of visible light irradiation, the azophenyl group will undergo reversible changes, from the cis isomer to the trans isomer again, resulting in the re-emulsification of the system.

3.5. Photoresponsive phase transfer emulsion of FADC-4/ n-octanol/water system

In addition to emulsification-demulsification, it was found that phase transfer could occur in a **FADC-4**/n-octanol/water emulsion system due to the weak solvent effect of n-octanol on **FADC-4**. As shown in Figure 11a, after UV irradiation, **FADC-4** changed from its *trans* to *cis* configuration, becoming more hydrophilic. This caused **FADC-4** to transfer from the n-octanol phase to the water phase, resulting in the n-octanol phase becoming lighter in color and the water phase becoming darker. Upon irradiation with 445 nm blue light, **FADC-4** reverted to its trans configuration and transferred back from the water phase to the n-octanol phase. The actual experimental pictures are showing in Figure 11b.

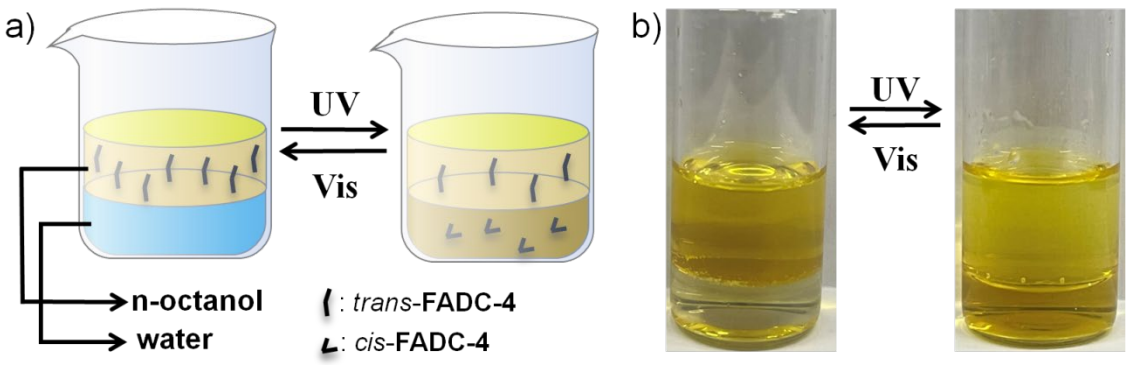

Figure 11. a) After UV irradiation, **FADC-4** transitioned from *trans* to *cis*, becoming more hydrophilic and transferring from the n-octanol phase to the water phase, resulting in a change in phase colors. Upon 445 nm blue light irradiation, **FADC-4** reverted to its *trans* configuration and transferred back to the n-octanol phase; b) Actual experimental images of the **FADC-4** phase transfer phenomena.

4. Conclusion

In conclusion, this study successfully prepared and characterized two photoresponsive molecules with three emulsion systems (**FADC-2**/n-hexane/water, **FADC-4**/n-hexane/water, and **FADC-4**/n-octanol/water), demonstrating significant potential for practical applications. The photoresponse stability of both **FADC-2**/n-hexane/water and **FADC-4**/n-hexane/water systems was firstly examined, showing that higher surfactant concentrations hinder demulsification, while longer carbon chains enhance stability. Then, the **FADC-2**/n-hexane/water emulsion system was further confirmed as an oil-in-water emulsion, with its phase diagram establishing the stable emulsion ratio. Optical microscopy revealed that UV irradiation increased the average emulsion size from 2.55 μm to 3 μm, indicating a transition from the oil-in-water region to a two-phase system and demonstrating the photon-demulsification process. Additionally, a phase transfer **FADC-4**/n-octanol/water emulsion system was developed, capable of reversible surfactant transfer between the water and oil

phases. These findings underscore the effectiveness of photoresponsive surfactants in controlled emulsion systems, offering promising applications in fields requiring precise emulsion manipulation and phase transfer capabilities, such as potential applications in controlled light release systems, separation and purification, etc. Despite the great potential of photoresponsive smart emulsions, many challenges remain for practical applications, such as improving the response speed to light, enhancing emulsion stability, and ensuring the photostability of photosensitive molecules. However, with advances in materials science and chemical synthesis, it is anticipated that new smart photoresponsive emulsions will continue to emerge and play a significant role in fields like healthcare, environmental monitoring, energy, and advanced manufacturing.

5. Acknowledgements

This work was supported by the Key Technology and Industrial Application Demonstration Project of High Quality and High Purity Nano Calcium Carbonate of Guangxi Province (Grant No. 17202030-2), the Gansu Province Key Research and Development Program (Grant No. 23YFGA0044) and the Innovation Fund of Small and Medium-sized Enterprises of Gansu Province (Grant No. 1407GCCA013).

6. Conflict of interest

The authors declare that they have no conflict of interest.

7. Author contributions

Conceptualization: Nong Wang, Zhihang Wang

Formal analysis: Hongyan Xue, Youmei Han

Investigation: Hongyan Xue, Youmei Han, Guanglei Liu

Methodology: Nong Wang, Wenjing Chen

Resources: Nong Wang

Writing – original draft: Nong Wang, Hongyan Xue, Zhihang Wang

Writing – review & editing: Nong Wang, Zhihang Wang

All authors have read and approved the final version to be published. '

8. References

[1] S. Ghosh, A. Ray, N. Pramanik, Self-assembly of surfactants: An overview on general aspects of amphiphiles, Biophysical Chemistry, 265 (2020) 106429.

[2] A.D.W. Carswell, E.A. O'Rea, B.P. Grady, Adsorbed Surfactants as Templates for the Synthesis of Morphologically Controlled Polyaniline and Polypyrrole Nanostructures on Flat Surfaces: From Spheres to Wires to Flat Films, Journal of the American Chemical Society, 125 (2003) 14793-14800.

[3] S. Liu, X. Wang, Q. Yin, X. Xiang, X.-Z. Fu, X.-Z. Wang, J.-L. Luo, A facile approach to fabricating graphene/waterborne epoxy coatings with dual functionalities of barrier and corrosion inhibitor, Journal of Materials Science & Technology, 112 (2022) 263-276.

[4] F.M. Menger, J.S. Keiper, Gemini Surfactants, Angewandte Chemie International Edition, 39 (2000) 1906-1920.

[5] Y. Liu, P.G. Jessop, M. Cunningham, C.A. Eckert, C.L. Liotta, Switchable Surfactants, Science, 313 (2006) 958-960.

[6] S. Polarz, M. Kunkel, A. Donner, M. Schlötter, Added-Value Surfactants, Chemistry – A European Journal, 24 (2018) 18842-18856.

[7] Y. Kazemzadeh, I. Ismail, H. Rezvani, M. Sharifi, M. Riazi, Experimental investigation of stability of water in oil emulsions at reservoir conditions: Effect of ion type, ion concentration, and system pressure, Fuel, 243 (2019) 15-27.

[8] Y. Kazemzadeh, H. Rezvani, I. Ismael, M. Sharifi, M. Riazi, An experimental study toward possible benefits of water in oil emulsification in heavy oil reservoirs: comparing role of ions and nanoparticles, Materials Research Express, 6 (2019) 085702.

[9] S. Mohammadreza Shams, Y. Kazemzadeh, M. Riazi, F.B. Cortés, Effect of pressure on the optimal salinity point of the aqueous phase in emulsion formation, Journal of Molecular Liquids, 362 (2022) 119783.

[10] X.-h. Ge, L. Mo, A. Yu, C. Tian, X. Wang, C. Yang, T. Qiu, Stimuli-responsive emulsions: Recent advances and potential applications, Chinese Journal of Chemical Engineering, 41 (2022) 193-209.

[11] L. Kong, S. Zhu, X. Quan, Y. Peng, Effect of phenyl functional group on the demulsification process of dodecyl anion emulsified asphalt, Construction and Building Materials, 354 (2022) 129196.

[12] G. Sun, Z. Li, T. Ngai, Inversion of Particle-Stabilized Emulsions to Form High-Internal-Phase Emulsions, Angewandte Chemie International Edition, 49 (2010) 2163-2166.

[13] J. Jiang, S. Yu, W. Zhang, H. Zhang, Z. Cui, W. Xia, B.P. Binks, Charge-Reversible Surfactant-Induced Transformation Between Oil-in-Dispersion Emulsions and Pickering Emulsions, Angewandte Chemie International Edition, 60 (2021) 11793-11798.

[14] Y. Xi, B. Liu, H. Jiang, S. Yin, T. Ngai, X. Yang, Sodium caseinate as a particulate emulsifier for making indefinitely recycled pH-responsive emulsions, Chemical Science, 11 (2020) 3797-3803.

[15] Y. Xu, Y. Zhang, X. Liu, H. Chen, Y. Fang, Retrieving Oil and Recycling Surfactant in Surfactant-Enhanced Soil Washing, ACS Sustainable Chemistry & Engineering, 6 (2018) 4981-4986.

[16] J. Wu, X. Guan, C. Wang, T. Ngai, W. Lin, pH-Responsive Pickering high internal phase emulsions stabilized by Waterborne polyurethane, Journal of Colloid and Interface Science, 610 (2022) 994-1004.

[17] L. Liu, M. Zhang, Z. Lu, Z. Jin, Y. Lu, D. Sun, Z. Xu, Molecular structure-tuned stability and switchability of CO2-responsive oil-in-water emulsions, Journal of Colloid and Interface Science, 627 (2022) 661-670.

[18] Y. Wang, L. Zhu, H. Zhang, H. Huang, L. Jiang, Formulation of pH and temperature dual-responsive Pickering emulsion stabilized by chitosan-based microgel for recyclable biocatalysis, Carbohydrate Polymers, 241 (2020) 116373.
[19] H. Zhang, L. Ge, C. Ding, R. Guo, Magnetic response Janus emulsions stabilized by Mangeto-surfactant, Journal of Molecular Liquids, 349 (2022) 118416.
[20] M. Reifarth, M. Bekir, A.M. Bapolisi, E. Titov, F. Nußhardt, J. Nowaczyk, D. Grigoriev, A. Sharma, P. Saalfrank, S. Santer, M. Hartlieb, A. Böker, A Dual pH- and Light-Responsive Spiropyran-Based Surfactant: Investigations on Its Switching Behavior and Remote Control over Emulsion Stability, Angewandte Chemie International Edition, 61 (2022) e202114687.
[21] Z. Li, Y. Shi, A. Zhu, Y. Zhao, H. Wang, B.P. Binks, J. Wang, Light-Responsive, Reversible Emulsification and Demulsification of Oil-in-Water Pickering Emulsions for Catalysis, Angewandte Chemie International Edition, 60 (2021) 3928-3933.
[22] S. Zhou, K. Sheng, N. Zhang, S. Yuan, N. Feng, Y. Song, J. Geng, X. Xin, Reversible demulsification and emulsification of surfactant emulsions regulated by light-responsive azo functionalized copper nanoclusters, Journal of Molecular Liquids, 367 (2022) 120384.
[23] J.-L. Guo, Q.-Q. Sun, Z.-Q. Liu, F.-X. Wang, T. Fu, Y. Liu, A. Ying, An intelligent dual stimuli-responsive Pickering emulsion for highly efficiently producing waste frying oil-based biodiesel, Journal of Cleaner Production, 436 (2024) 140638.
[24] H.-X. Yu, X. Yu, S. Chen, J. Hao, L. Xu, A monosurfactant-stabilized dual-responsive and versatile emulsion lubricant, Journal of Cleaner Production, 406 (2023) 137089.
[25] Z. Mahimwalla, K.G. Yager, J.-i. Mamiya, A. Shishido, A. Priimagi, C.J. Barrett, Azobenzene photomechanics: prospects and potential applications, Polymer Bulletin, 69 (2012) 967-1006.
[26] Z. Wang, R. Losantos, D. Sampedro, M.-a. Morikawa, K. Börjesson, N. Kimizuka, K. Moth-Poulsen, Demonstration of an azobenzene derivative based solar thermal energy storage system, Journal of Materials Chemistry A, 7 (2019) 15042-15047.
[27] Y. Zhou, H. Ye, Y. Chen, R. Zhu, L. Yin, Photoresponsive Drug/Gene Delivery Systems, Biomacromolecules, 19 (2018) 1840-1857.
[28] B.R. Smith, S.S. Gambhir, Nanomaterials for In Vivo Imaging, Chemical Reviews, 117 (2017) 901-986.
[29] Q. Zhang, H. Wang, L. Qiu, X. Han, Z. Wang, N. Wang, Synthesis and Characteristics of Smart Coating Materials for Reversible Double Stimulus-Responsive Oil–Water Separation, ACS Applied Polymer Materials, 6 (2024) 6482-6494.
[30] P. Zhang, F. Cai, W. Wang, G. Wang, H. Yu, Light-Switchable Adhesion of Azobenzene-Containing Siloxane-Based Tough Adhesive, ACS Applied Polymer Materials, 3 (2021) 2325-2329.
[31] X. Zheng, Y. Jia, A. Chen, Azobenzene-containing liquid crystalline composites for robust ultraviolet detectors based on conversion of illuminance-mechanical stress-electric signals, Nature Communications, 12 (2021) 4875.
[32] E. Merino, Synthesis of azobenzenes: the coloured pieces of molecular materials, Chemical Society Reviews, 40 (2011) 3835-3853.
[33] L. Song, R. Wang, K. Niu, Y. Liu, J. Kou, H. Song, J. Zhang, Q. Wang, Design, synthesis, characterization, and surface activities of comb-like polymeric fluorinated surfactants with short fluoroalkyl chains, Colloids and Surfaces A: Physicochemical and Engineering Aspects, 609 (2021) 125666.
[34] F. Zhao, Z. Jing, X. Guo, J. Li, H. Dong, Y. Tan, L. Liu, Y. Zhou, R. Owen, P.R. Shearing, D.J.L. Brett, G. He, I.P. Parkin, Trace amounts of fluorinated surfactant additives enable high performance zinc-ion batteries, Energy Storage Materials, 53 (2022) 638-645.
[35] Y. Pei, J. Ma, F. Song, Y. Zhao, Z. Li, H. Wang, J. Wang, R. Du, Stable nanoreactors for material fabrication using the aggregation of fluorinated ionic liquid surfactants in ionic liquid solvents, Journal of Molecular Liquids, 366 (2022) 120256.
[36] C. Hill, A. Czajka, G. Hazell, I. Grillo, S.E. Rogers, M.W.A. Skoda, N. Joslin, J. Payne, J. Eastoe, Surface and bulk properties of surfactants used in fire-fighting, Journal of Colloid and Interface Science, 530 (2018) 686-694.
[37] G.M.C. Silva, P. Morgado, E.J.M. Filipe, Towards compartmentalized micelles: Mixed perfluorinated and hydrogenated ionic surfactants in aqueous solution, Journal of Colloid and Interface Science, 654 (2024) 906-914.
[38] S. Peshoria, D. Nandini, R.K. Tanwar, R. Narang, Short-chain and long-chain fluorosurfactants in firefighting foam: a review, Environmental Chemistry Letters, 18 (2020) 1277-1300.
[39] K. Qiu, X. Yu, H. Li, S. Lu, Tuning rheology and fire-fighting performance of protein-stabilized foam by actively switching the interfacial state of the liquid film, Journal of Materials Science & Technology, 178 (2024) 120-132.

[40] R. Wang, X. Xu, X. Shi, J. Kou, H. Song, Y. Liu, J. Zhang, Q. Wang, Promoting Efficacy and Environmental Safety of Pesticide Synergists via Non-Ionic Gemini Surfactants with Short Fluorocarbon Chains, Molecules, 27 (2022) 6753.
[41] X. Yu, F. Li, H. Fang, X. Miao, J. Wang, R. Zong, S. Lu, Foaming behavior of fluorocarbon surfactant used in fire-fighting: The importance of viscosity and self-assembly structure, Journal of Molecular Liquids, 327 (2021) 114811.
[42] S. Gao, Z. Cao, Q. Niu, W. Zong, R. Liu, Probing the toxicity of long-chain fluorinated surfactants: Interaction mechanism between perfluorodecanoic acid and lysozyme, Journal of Molecular Liquids, 285 (2019) 607-615.
[43] C.A. Moody, J.A. Field, Perfluorinated Surfactants and the Environmental Implications of Their Use in Fire-Fighting Foams, Environmental Science & Technology, 34 (2000) 3864-3870.
[44] A.V. Alves, M. Tsianou, P. Alexandridis, Fluorinated Surfactant Adsorption on Mineral Surfaces: Implications for PFAS Fate and Transport in the Environment, Surfaces, 3 (2020) 516-566.
[45] A. Zaggia, B. Ameduri, Recent advances on synthesis of potentially non-bioaccumulable fluorinated surfactants, Current Opinion in Colloid & Interface Science, 17 (2012) 188-195.
[46] E.-k. Kang, G.Y. Jung, S.H. Jung, B.M. Lee, Synthesis and surface active properties of novel anionic surfactants with two short fluoroalkyl groups, Journal of Industrial and Engineering Chemistry, 61 (2018) 216-226.
[47] R. Zhou, Y. Jin, Y. Shen, S. Lai, Y. Zhou, P. Zhao, Surface activity, salt and pH tolerance, and wettability of novel nonionic fluorinated surfactants with a short fluorocarbon chain, Journal of Dispersion Science and Technology, 42 (2020) 152-159.
[48] D.R. Meena, S.R. Gadre, P. Balanarayan, PAREMD: A parallel program for the evaluation of momentum space properties of atoms and molecules, Computer Physics Communications, 224 (2018) 299-310.
[49] C. Wallace, K. Griffiths, B.L. Dale, S. Roberts, J. Parsons, J.M. Griffin, V. Görtz, Understanding Solid-State Photochemical Energy Storage in Polymers with Azobenzene Side Groups, ACS Applied Materials & Interfaces, 15 (2023) 31787-31794.
[50] Y. Kazemzadeh, M. Sharifi, M. Riazi, Optimization of Fe3O4/Chitosan nanocomposite concentration on the formation and stability of W/O emulsion, Materials Research Express, 6 (2019) 035031.
[51] S.M. Shams, A.A. Dehghan, Y. Kazemzadeh, M. Riazi, Experimental investigation of emulsion formation and stability: Comparison of low salinity water and smart water effect, Journal of Dispersion Science and Technology, 45 (2024) 1646-1655.
[52] H. Garmsiri, S. Jahani, Y. Kazemzadeh, M. Sharifi, M. Riazi, R. Azin, Stability of the emulsion during the injection of anionic and cationic surfactants in the presence of various salts, Scientific Reports, 13 (2023) 11337.
[53] M. Mohammadpour, M.R. Malayeri, Y. Kazemzadeh, M. Riazi, On the impact of oil compounds on emulsion behavior under different thermodynamic conditions, Scientific Reports, 13 (2023) 15727.